CRYSTAL GROWTH & DESIGN

pubs.acs.org/crystal

Article



# Extensive Screening and Performance Testing of Nucleating Agents for the Sodium Acetate Trihydrate Phase-Change Material

Jinjie Li, Michael A. Parkes, and Christoph G. Salzmann*

Cite This: *Cryst. Growth Des.* 2024, 24, 8292−8300

Read Online

ACCESS | Metrics & More | Article Recommendations | Supporting Information

**ABSTRACT:** Heat batteries often rely on phase-change materials that undergo phase transitions upon heat charging and release. Sodium acetate trihydrate (SAT) is considered to be one of the best phase-change materials in terms of storage capacity. Yet, it is well-known for supercooling, which makes the search for effective nucleating agents a high priority. To perform extensive screening of nucleating agents and to test their performance, we designed a new instrument. The HeatMaster is capable of analyzing six samples on the gram-scale in parallel using the principle of power compensation, which means that heat releases and uptakes can be obtained in a quantitative fashion. Out of the 36 tested nucleating agents, $CaCl_2{\cdot}2H_2O$ was identified as the best nucleating agent that outperforms several of the previously known nucleating agents in terms of temperature range of operation up to 80 °C. $CaCl_2{\cdot}2H_2O$ performs reliably as a nucleating agent for SAT down to 0.5 wt %. $MgCl_2{\cdot}6H_2O$ was also identified as a nucleating agent. Yet, similar to the well-known $Na_2HPO_4{\cdot}12H_2O$, its performance is not reliable after heating to 80 °C. Out of the three nucleating agents, $CaCl_2{\cdot}2H_2O$ shows the best performance with respect to deterioration of the heat releases upon extensive thermal cycling with a maximum temperature of 65 °C.

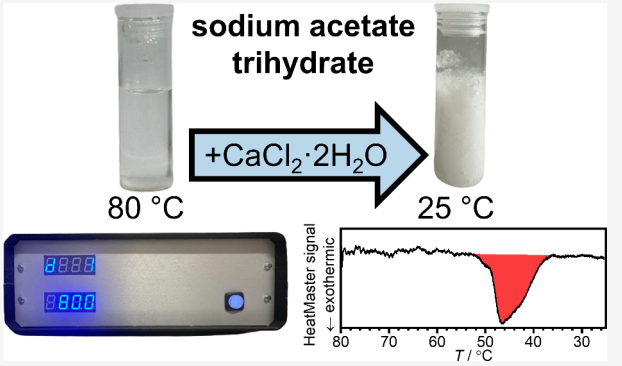




## INTRODUCTION

Heat batteries are important devices for storing thermal energy from heat pumps, solar and wind sources, off-peak electricity, and industrial-waste heat.[1−7] Typically, the heat charging and release are achieved with the help of phase-change materials that undergo reversible phase transitions. A wide variety of phase-change materials have been employed successfully including metal alloys, paraffins, fatty acids, sugar alcohols, ionic liquids, and salt hydrates.[1,4,5,8] Commercially viable phase-change materials should be cheap, display high-energy densities, and release heat at a temperature suited for the application. Furthermore, their performance should remain as constant as possible during the lifetime of a heat battery. Compared to electrical batteries, heat batteries typically do not require expensive raw materials for their manufacture, such as lithium and cobalt, which is important for sustainability and environmental aspects.

Salt hydrates have received much attention as phase-change materials due to their high energy densities as well as low price, flammability, and toxicity.[5,9−11] They are considered the best heat-storage materials with heat densities of up to 514 MJ $m^{-3}$.[12] The heat uptake or release are observed at the melting points of the salt hydrates. A drawback associated with salt hydrates is their low thermal conductivity, which can be addressed by creating composites with materials providing higher thermal conductivities.[9,13] Liquid salt hydrates also often supercool, which means that the heat releases are either delayed or not observed at all.[9] This problem can be addressed by adding appropriate nucleating agents. However, the search for effective nucleating agents is typically conducted on a trial and error basis, and the performance of nucleating agents may degrade over time.[14]

Incongruent melting of salt hydrates can also be problematic. This means that a salt hydrate melts to give a precipitate of its anhydrate or a hydrate with lower water content in addition to the liquid phase, which consequently has a different chemical composition compared to the original hydrate.[9] Such effects can lead to phase separation, difficulties with rehydration upon heat release, and ultimately performance losses of the heat batteries.[15] These problems can be minimized by mechanical agitation,[16] addition of thickeners,[17−20] and microencapsulation.[21,22] A further requirement for phase-change materials is a small volume change upon crystallization, which would otherwise subject the heat batteries to undesirable mechanical stresses.[14,23] A general

Received: May 23, 2024
Revised: September 10, 2024
Accepted: September 11, 2024
Published: September 26, 2024

disadvantage of salt hydrates is their corrosive nature, which means that leakages from heat batteries must be avoided.[24]

Sodium acetate trihydrate (SAT) is a popular salt hydrate that is used widely in commercial heat batteries and is well-known from its use in handwarmers.[25] It releases 226−264 J $g^{-1}$ at a melting point of 58 °C, which is a convenient temperature for domestic heating and hot tap water.[26−31] As can be seen in Figure 1, SAT melts incongruently to give a

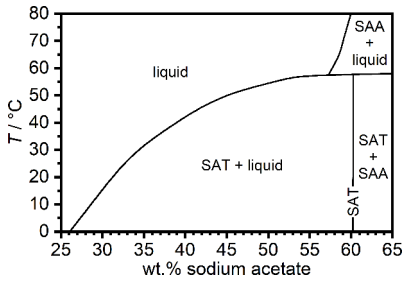


**Figure 1.** Binary phase diagram of sodium acetate and water, including areas of stability of sodium acetate trihydrate (SAT) and sodium acetate anhydrate (SAA). Adapted from refs 29 and 32.

liquid solution and solid sodium acetate anhydrate (SAA). Oliver et al. showed that specific polymer additives can suppress and even prevent the SAA formation.[27] The peritectic point of SAT and SAA is found at about 57 wt %.

SAT is well-known for extensive supercooling.[14,25] Yet, a variety of nucleating agents for SAT have been identified. These include $Na_4P_2O_7{\cdot}10H_2O$,[27,31,33] sodium hydrogen phosphates such as $Na_2HPO_4$, $Na_2HPO_4{\cdot}2H_2O$, $Na_2HPO_4{\cdot}7H_2O$, and $Na_2HPO_4{\cdot}12H_2O$,[17,18,27,34] $K_2SO_4$,[35] $Al_2O_3$,[36] nanocopper (10−30 nm),[37] silver nanoparticles,[38] AlN nanoparticles,[39] silicon carbide and bentonite,[40] activated charcoal,[41] expanded graphite,[19] and chitin nanowhiskers.[42] Why certain materials nucleate SAT is unclear, and it is also not well-understood why some materials become inactive upon heating to just a few tens of degrees above the melting point of SAT. An exception is the work by Oliver et al., who demonstrated that as $Na_2HPO_4{\cdot}2H_2O$ undergoes thermally induced dehydration, it becomes inactive as a nucleating agent.[27] Another concern is that an initially active nucleating agent may fail to work upon extensive thermal cycling over the lifetime of a heat battery.[43]

Inducing crystallization is, in general, a difficult process, as pure liquids and solutions often supercool. According to classical nucleation theory (CNT), a nucleus of crystalline material with a certain critical size needs to form so that the nucleation event is followed by crystal growth. For solutions, the two-step model suggests that clusters of dense liquid need to form first before crystallization can begin within these clusters.[44] For many materials, nucleation is difficult to achieve in the liquid phase. Instead, nucleation and subsequent crystal growth often take place at heterogeneous liquid/solid interfaces. It is important that the solid particles are larger than the size of the critical nucleus.[45] While simple concepts such as a match of lattice constants sometimes apply,[46] it is often unclear which structures at the interfaces act as the nucleation sites.[47] In many cases, defect structures that are different compared to the bulk structure of the nucleating agent may be responsible for inducing nucleation.[48]

Differential scanning calorimetry (DSC) is often used for characterizing the supercooling and heat releases of phase-change materials. Yet, the amount of sample is typically only several tens of milligrams, which is several orders of magnitude away from heat-battery applications. This means that supercooling effects and the problems associated with incongruent melting may not be captured reliably.[30] Commercial DSCs can also typically measure only one sample at a time.

Gram-scale measurements of phase-change materials often only measure the thermal history of samples.[42] This means that the sample temperature is recorded while a sample is cooled below the melting point of SAT. Upon crystallization, the sample temperature "jumps" to the temperature of the melting point, and further cooling is only observed once the sample has fully crystallized. Determining the heat release from such a setup in a quantitative fashion is difficult, and it is not possible to enforce defined cooling rates.[42] On the plus side, due to the simplicity of the measurement, it is quite straightforward to conduct several experiments at the same time.

The Galisol instrument contains about 10 g of a single phase-change material and can determine the latent heats of crystallization through careful calibration of the heat capacities of the various parts of the instrument.[14] Large individual samples can also be analyzed using three-layer calorimetry[49] and Peltier-element-based adiabatic scanning calorimetry.[50] Commercial reactors are also available, for example, from Cambridge Reactor Design and Mettler Toledo. These instruments can also handle sample sizes well beyond the DSC scale yet typically measure only one or two samples at most at a time.

Here we design an instrument that is capable of characterizing six phase-change materials on the gram-scale in parallel using the principle of power compensation. In addition to melting/crystallization temperatures, the heat uptakes/releases are determined in a quantitative fashion without the need for calibrating calorimeter parts with respect to their heat capacities. The design is easily scalable at low cost and could include substantially more than six calorimeters running in parallel. Using the new instrument, we aim to identify new nucleating agents for SAT and to test their performance upon extensive thermal cycling.

## EXPERIMENTAL SECTION

**Design of the HeatMaster Instrument.** A bespoke instrument for thermal cycling and performance testing of phase-change materials was built. Our HeatMaster instrument characterizes six gram-scale samples in parallel and determines the heat releases or uptakes associated with phase transitions in a quantitative fashion. A photograph of the entire setup and a schematic drawing of one of the six heating modules are shown in Figure 2(a) and (b), respectively. The heating modules (1) were machined from 40 × 40 × 55 mm aluminum blocks. A central cylindric cavity (2) accepts 10 mL glass vials (Samco soda glass specimen tubes with stopper 16 × 50 mm) containing the phase-change materials. The temperature of the aluminum block is measured close to the sample vial with a (3) Pt100 sensor in 4-wire configuration (RS Components, RS PRO PT100 RTD sensor, 2.8 mm diameter, 15 mm long, class A). The aluminum block is heated with (4) two resistive heating elements (Makers Hut, 24 V, 60 W, 6 × 20 mm ceramic cartridge heater) connected in parallel to a DC power supply with RS232 serial port (Tenma, model 72-2540, 30 V, 5 A). Two M6 screws were inserted into the (5) holes of the aluminum blocks to firmly attach the heating modules to a (6) water-cooled aluminum cold sink separated by (7) 0.5 mm thick Teflon spacers.

The controller box of the HeatMaster contains one Adafruit Feather M0 Proto microcontroller for each of the six heating modules. The code for the various microcontrollers was written in C++ in the


https://doi.org/10.1021/acs.cgd.4c00691
Cryst. Growth Des. 2024, 24, 8292−8300

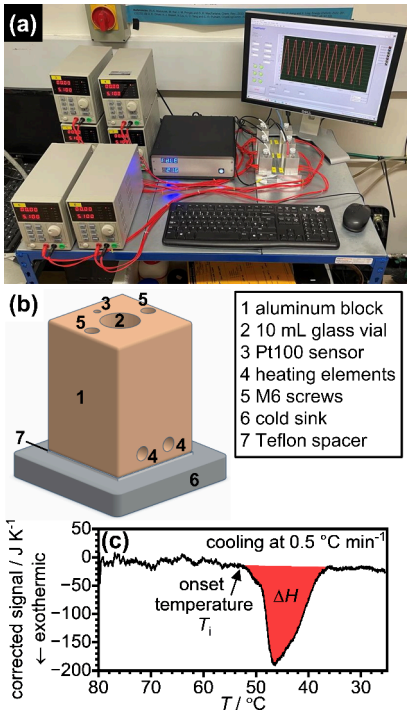


**Figure 2.** (a) Photographic image of the HeatMaster instrument. (b) Schematic rendering of one of the six heating modules with the locations of the various additional components indicated. (c) Background-corrected HeatMaster signal recorded upon cooling 5 g of sodium acetate trihydrate with nucleating agent at 0.5 °C $min^{-1}$ from 80 to 25 °C. The exotherm due to the crystallization of sodium acetate trihydrate is shown as a red-shaded area, and the onset temperature of crystallization, $T_i$, is indicated with an arrow.

Arduino IDE. Specifically, the six microcontrollers were programmed to read the temperatures of the heating modules using Adafruit MAX31865 Pt100 amplifiers, to set the voltages of the power supplies via TTL-RS232 converters, and to read the electric currents from the power supplies. Each microcontroller can accept a set point temperature, which is then realized using a PID control algorithm with the Pt100 temperature as the input and the voltage of the power supply as output (0–20 V).

An additional Adafruit Feather M0 acted as the master microcontroller and controlled the six microcontrollers responsible for the individual heating modules. Within the master microcontroller, a temperature program is defined in terms of four stages including (1) dwelling at a base temperature for a specified period of time, (2) heating at a defined heating rate, (3) dwelling at the maximum temperature for a specified period of time, and (4) cooling back to the base temperature at a defined cooling rate. These four stages constitute a cycle and can be repeated until a total number of specified cycles is reached. The set point temperatures from a defined temperature profile are sent to the six microcontrollers every second, and the voltages and currents required to follow the temperature profile are returned to the master microcontroller as well as the actual temperatures. Figure S1(a) shows the temperature profile of a typical experiment with 10 cycles, a base temperature of 25 °C, a maximum temperature of 80 °C, 0.5 °C $min^{-1}$ as heating/cooling rates and using empty glass vials. The differences between the set point temperatures and the actual temperatures of the six modules are shown in Figure S1(b). It can be seen that the thermal lag upon heating and cooling is small and never exceeds 0.3 °C.

The electric power required to realize the temperature profile is calculated from the product of the voltage and current. Figure S2 shows the power profiles required to run the six heating modules according to the temperature profile shown in Figure S1(a). Power variations between the six modules are attributed to small variations in the thicknesses of the Teflon spacers and different proximities to the inlet of the cooling water on the cold sink.

For the heating and cooling stages, the electric power was divided by the heating/cooling rate, resulting in a signal with a unit of J $K^{-1}$, which can then be plotted against temperature. Figure S3 shows such data recorded upon cooling an empty vial as well as a vial containing 5 g of SAT with a nucleating agent from 80 to 25 °C at 0.5 °C $min^{-1}$. As the sample releases heat upon crystallization, the PID algorithm regulates back the voltage of the heating element so that the temperature profile is followed as closely as possible. This results in a negative deviation of the signal compared to the empty vial, as highlighted by the arrow in Figure S3. The resulting exothermic feature is more clearly seen once the signal of the empty vial is subtracted as a background, as shown in Figure 2(c). To improve the noise levels, the empty-vial data were fitted with a polynomial function for the subtraction with a Python script. The resulting exothermic feature can then be integrated to obtain the crystallization enthalpy, $\Delta H$, and the onset temperature of crystallization, $T_i$, can be determined, as indicated by the arrow. The successful power compensation achieved by the PID algorithm during crystallization can be seen from the small temperature differences upon cooling an empty glass vial, and a vial containing 5 g of SAT and nucleating agent in Figure S4.

Figure S5(a) shows the background-corrected cooling curves for vials containing different amounts of SAT ranging from 5 to 1 g. The obtained crystallization enthalpies are plotted against the mass of SAT in Figure S5(b). It can be seen that the HeatMaster shows a good linear response, and the crystallization enthalpy per gram of SAT determined from the slope in Figure S5(b) is −202.9 ± 8.4 J $g^{-1}$, which agrees with the values reported in the literature.[26−31] Additionally, the HeatMaster was tested with phenyl salicylate, which is a well-known reference material in calorimetry.[51] We obtained an onset melting temperature of 41.0 ± 0.9 °C and a melting enthalpy of 97.3 ± 7.6 J $g^{-1}$. This agrees well with the literature values of 41.9 ± 0.5 °C and 90 ± 3 J $g^{-1}$.[51] The LGC Certified Reference Material values are 41.79 °C and 89.53 J $g^{-1}$.

As a safety feature, the master microcontroller also monitors the temperature of the cold sink and is programmed to immediately stop any heating of the six modules should the temperature exceed 30 °C.

Finally, a LabView program on a PC sends all of the required experimental parameters to the master microcontroller to initiate a measurement, and it receives and records the actual temperatures of the modules as well as voltages and currents from each heating element over the course of the entire experiment. Our longest experiments so far lasted about 9 days with 50 temperature cycles.

**Sample Preparation for HeatMaster Experiments.** For a typical experiment, 5 g of SAT (Thermo Scientific, 99+%, extra pure) and 0.25 g (4.76 wt %) of a potential nucleating agent were placed in a sample vial and thoroughly shaken. The vial was then sealed with PTFE tape around the plastic stopper and inserted into the HeatMaster. The standard heating profile involved thermal cycling between 25 and 80 °C at a rate of 0.5 °C $min^{-1}$, and dwelling times of 15 and 30 min at 25 and 80 °C, respectively. The maximum temperature was changed to 65 or 85 °C for some experiments.

**Powder X-ray Diffraction.** The samples formed hard, monolithic blocks of material inside the glass vials after crystallization, which made recovery very difficult. Using a face shield and leather gloves, the glass vials were carefully broken with a hammer, and the samples were recovered as good as possible while carefully avoiding pieces of the broken glass. The recovered materials were ground with a pestle and mortar, and the powders were placed between greased acetate foils. X-ray diffraction patterns of the mounted samples were collected using a Stoe Stadi P X-ray diffractometer (Cu K$\alpha$1 radiation at 40 kV, 30 mA and monochromated by a Ge 111 crystal) equipped with a Mythen 1 K linear detector. The samples were rotated during the measurements, and diffraction patterns were collected over $2\theta$ = 2–60° with 0.5° steps and 5 s accumulation times per step. The GSAS software was used for Le Bail fitting of the diffraction patterns.[52]



https://doi.org/10.1021/acs.cgd.4c00691
Cryst. Growth Des. 2024, 24, 8292−8300

## RESULTS AND DISCUSSION

A total of 36 potential nucleating agents were tested with respect to their abilities to nucleate SAT upon cooling at 0.5 °C $min^{-1}$ from 80 °C. These included several water-insoluble materials such as graphite, kaolinite, $BaSO_4$, SiC, $CaCO_3$ (calcite), and ZnS. Yet, the majority of tested nucleating agents were various salts and salt hydrates, which may display some solubility in the molten SAT. For all experiments, 5 g of SAT was used as well as 0.25 g (4.76 wt %) of nucleating agent. The HeatMaster scans upon cooling are shown in Figure 3. Successful crystallization of SAT was observed only for two

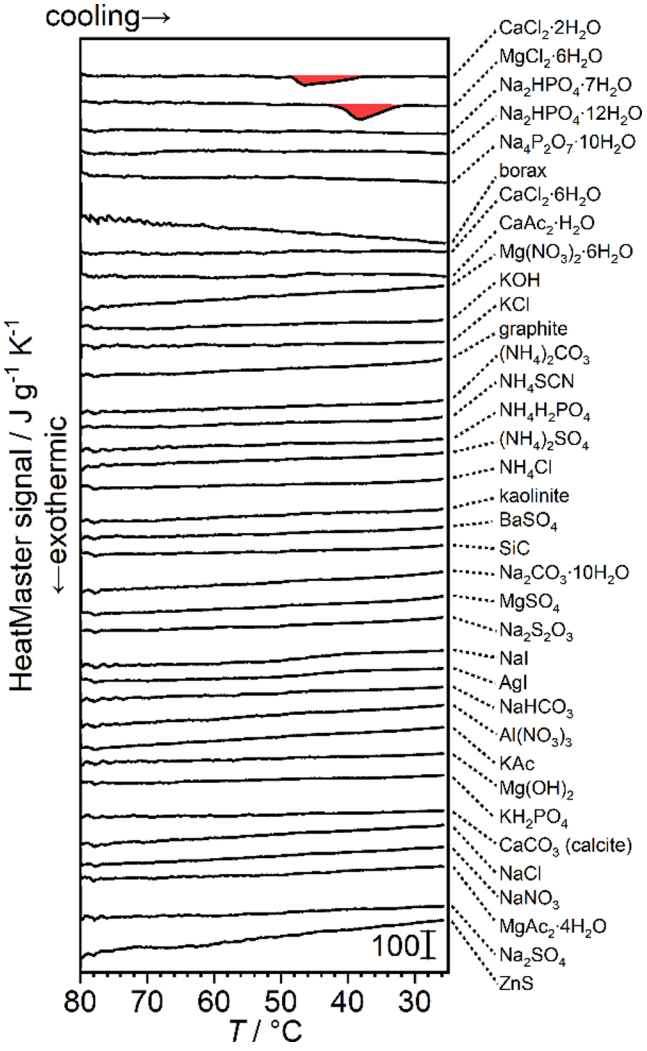


**Figure 3.** HeatMaster scans recorded upon cooling 5 g of sodium acetate trihydrate combined with 0.25 g (4.76 w%) of potential nucleating agent from 80 to 25 °C at 0.5 °C $min^{-1}$. The list of tested nucleating agents is given in the legend on the right-hand side of the figure. Crystallization exotherms were observed using $CaCl_2·2H_2O$ and $MgCl_2·6H_2O$ as nucleating agents, as indicated by the red-shaded exothermic peaks.

experiments using $CaCl_2·2H_2O$ and $MgCl_2·6H_2O$ as the nucleating agents. The crystallization exotherms are highlighted with red-shaded areas in Figure 3. To the best of our knowledge, these alkaline earth metal chloride hydrates have not yet been identified as nucleating agents for SAT. In all other cases, supercooling of the liquid SAT solutions was observed.

The reliability of $CaCl_2·2H_2O$ as a nucleating agent for SAT was tested in the next step. Figure 4 shows 10 heating/cooling cycles between 25 and 80 °C. The endothermic melting peaks are shown with a blue-shaded background in Figure 4(a). The first melting is shifted slightly toward higher temperatures, which can be attributed to a poorer thermal conductivity of the initially loose powder. Figure 4(b) shows that nucleation of SAT takes place reliably for all 10 cycles, as indicated by the red-shaded exotherms, and the reproducibility was confirmed with two additional samples also subjected to 10 heating/cooling cycles.

Upon reducing the amount of $CaCl_2·2H_2O$ from 0.250 g (4.76 w%) to 0.025 g (0.50 w%) while keeping the amount of SAT constant at 5 g, the crystallization exotherms continued to appear reliably, as shown in Figure 5. These tests were again conducted with three individual samples each subjected to 10 heating/cooling cycles. Upon lowering the amount of $CaCl_2·2H_2O$ to 0.005 g (0.10 w%), a slight shift of the exotherm toward lower temperatures was observed, indicating that $CaCl_2·2H_2O$ becomes somewhat less effective as a nucleating agent. Finally, at 0.001 g (0.02 wt %) of $CaCl_2·2H_2O$, no exotherms were observed during 10 heating/cooling cycles and for three individual samples. It seems likely that this small amount of $CaCl_2$ becomes soluble in liquid SAT and is, hence, no longer able to provide a solid interface for the nucleation of SAT upon cooling. Accordingly, the minimal amount of $CaCl_2·2H_2O$ needed for reliable nucleation of SAT is around 0.1 wt %. Yet 0.5 wt % is probably the best choice if supercooling needs to be minimized.

In contrast to $CaCl_2·2H_2O$, $MgCl_2·6H_2O$ is a less reliable nucleating agent upon cycling SAT between 25 and 80 °C, as shown in Figure 6 with heating scans in (a) and cooling scans in (b). Melting upon heating and crystallization upon cooling were observed only for the first two heating/cooling steps. After the third melting, the sample supercooled, as can be seen from cooling scan (3). During the fourth heating scan, cold crystallization of the metastable supercooled liquid was observed at around 40 °C, which was followed by melting above 50 °C. Upon cooling, all following cooling scans (4−10) show supercooling, and cold crystallization followed by melting was seen for heating scans (5) and (8). This data show that $MgCl_2·6H_2O$ cannot act as a reliable nucleating agent for SAT after a few heating/cooling cycles with a maximum temperature of 80 °C.

Using powder X-ray diffraction, it was confirmed that the starting material of all of our studies was pure SAT free from any contamination with SAA, as shown in Figure 7(a). The crystallization products after first cooling using $CaCl_2·2H_2O$ and $MgCl_2·6H_2O$ are also pure SAT (see Figure 7(b,c)). This is an important test since SAA can be a byproduct of crystallization, which degrades the performance of SAT as a phase-change material.[27] Due to the difficulties associated with the sample recovery from the glass vials (see Experimental Section), we assume that the nucleating agents remain attached to the broken pieces of glass, which would explain why they are not observed in the diffraction patterns in Figure 7(b,c).

When exotherms were absent upon cooling, the samples were sometimes found to contain some crystalline material at room temperature, which could turn the supercooled SAT solution into a viscous gel. In line with previous observations,[14] this crystalline material is presumably SAA, which crystallized without releasing detectable amounts of heat upon cooling.


https://doi.org/10.1021/acs.cgd.4c00691
Cryst. Growth Des. 2024, 24, 8292−8300

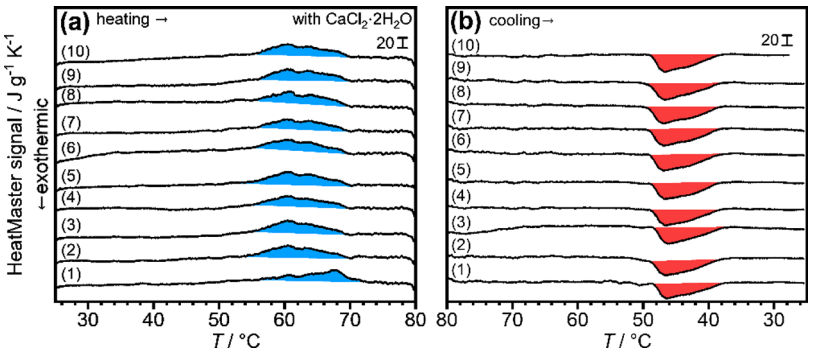


**Figure 4.** HeatMaster scans of 5 g of sodium acetate trihydrate with 0.25 g (4.76 w%) $CaCl_2·2H_2O$ and 10 cycles. (a) Heating at 0.5 °C min$^{-1}$ from 25 to 80 °C. (b) Cooling at 0.5 °C min$^{-1}$ from 80 to 25 °C. Endotherms and exotherms are indicated by blue- and red-shaded areas, respectively. The cycle numbers are given for each of the scans.

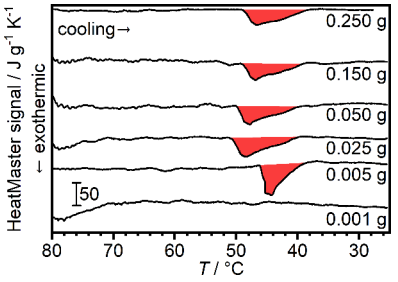


**Figure 5.** HeatMaster scans upon cooling 5 g of sodium acetate trihydrate with different masses of $CaCl_2·2H_2O$ as nucleating agent ranging from 0.250 (4.76 wt %) to 0.001 g (0.02 wt %). The cooling rate was 0.5 °C min$^{-1}$, and the crystallization exotherms are indicated by red-shaded areas.

Attempts to characterize this material with X-ray diffraction failed since opening the glass vials typically resulted in the crystallization of SAT, as noticed from the increase in temperature of the glass vials while holding them.

Reinspection of the data shown in Figure 3 raises the question why crystallization of SAT was not observed using $Na_2HPO_4·7H_2O$, $Na_2HPO_4·12H_2O$, and $Na_4P_2O_7·10H_2O$, which are well-known nucleating agents.[17,18,27,34] Closer analysis of the literature revealed that using 80 °C as the maximum temperature is quite harsh and that many of the known nucleating agents for SAT, including those based on sodium hydrogen phosphates, lose their performance at higher temperatures.[14,27] This has been attributed to the loss of SAT crystals on the surfaces of the nucleating agents.[29] Oliver et al. showed that $Na_2HPO_4·2H_2O$ becomes inactive above 72 °C due to thermally induced dehydration.[27]

As a test, we reduced the maximum temperature to 65 °C for the heating/cooling cycles and used 0.25 g (4.76 w%) of $Na_2HPO_4·12H_2O$ as the nucleating agent for 5 g of SAT. As shown in Figure S6, and consistent with the literature, $Na_2HPO_4·12H_2O$ was now indeed capable of inducing nucleation of SAT under these changed conditions. Equally, we found that the previously investigated $MgCl_2·6H_2O$ (see Figure 6) becomes a reliable nucleating agent when a maximum temperature of 65 °C is used, as shown in Figure S7.

It can be concluded that $CaCl_2·2H_2O$ is an excellent nucleating agent for SAT that performs well, unlike other nucleating agents, under quite harsh temperature conditions up to 80 °C. This could be a technological advantage since accidental heating of heat batteries containing other nucleating agents could effectively render them inactive.

To test the temperature limits of the ability of $CaCl_2·2H_2O$ for nucleating SAT, the crystallization experiments were performed with an upper dwelling temperature of 85 °C as the next step. It can be seen in Figure S8, that $CaCl_2·2H_2O$ begins to fail nucleating SAT after the second cooling step, which means that $CaCl_2·2H_2O$ becomes inactive after spending some time at 85 °C. In comparison, $MgCl_2·6H_2O$ became inactive during dwelling at 80 °C. $CaCl_2·2H_2O$ is stable up to 175 °C,[60,61] whereas $MgCl_2·6H_2O$ dehydrates at 116 °C.[62,63] This means that in both cases dehydration does not seem to be the cause for the diminishing nucleating abilities at higher temperatures. It can be speculated that the higher temperatures may remove surface defects responsible

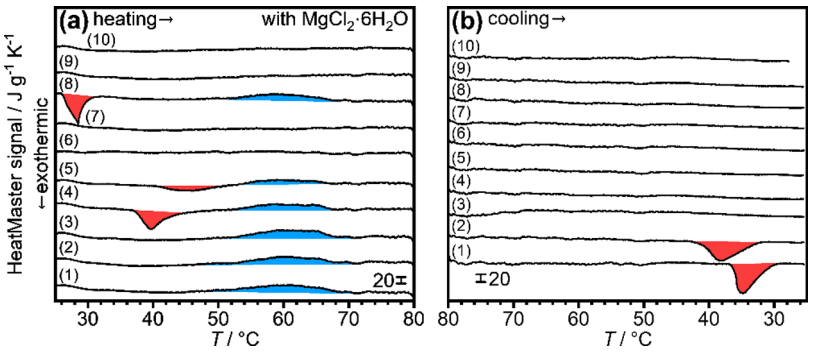


**Figure 6.** HeatMaster scans of 5 g of sodium acetate trihydrate with 0.25 g (4.76 wt %) of $MgCl_2·6H_2O$ and 10 cycles. (a) Heating at 0.5 °C min$^{-1}$ from 25 to 80 °C. (b) Cooling at 0.5 °C min$^{-1}$ from 80 to 25 °C. Endotherms and exotherms are indicated by blue- and red-shaded areas, respectively.



https://doi.org/10.1021/acs.cgd.4c00691
Cryst. Growth Des. 2024, 24, 8292−8300

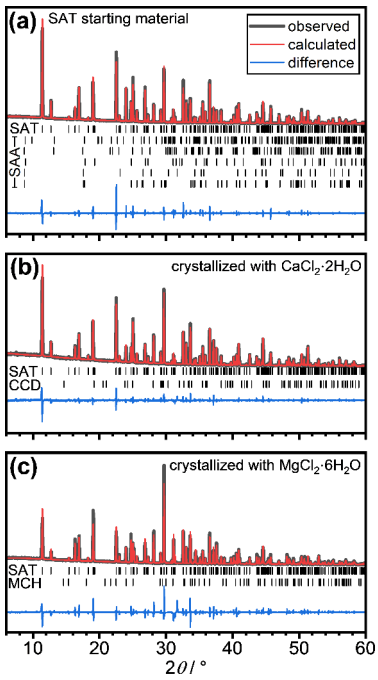


**Figure 7.** Power X-ray diffraction patterns (Cu K$\alpha$) of (a) the sodium acetate trihydrate starting material and sodium acetate trihydrate crystallized using (b) $CaCl_2·2H_2O$ and (c) $MgCl_2·6H_2O$ as nucleating agents. Experimental data are shown as black lines, Le Bail fits are shown as red lines, and difference curves are in blue. Tick marks indicate the expected positions of Bragg peaks of sodium acetate trihydrate (SAT),[53,54] various sodium acetate anhydrate (SAA) polymorphs,[55−57] $CaCl_2·2H_2O$ (CCD),[58] and $MgCl_2·6H_2O$ (MCH).[59]

for nucleation or that the crystal morphologies change so that the active crystal surfaces are no longer present. The fact that $MgCl_2·6H_2O$ and $CaCl_2·2H_2O$ remain active at 80 and 85 °C, respectively, for a few cycles, including 30 min dwelling times at the maximum temperatures, suggests that the kinetics of the degradation reactions are relatively slow, which would be consistent with defect annealing or morphology changes.

Regarding the molecular details of the nucleation event at the interfaces of $CaCl_2·2H_2O$ or $MgCl_2·6H_2O$ with liquid SAT, it can be speculated that the carboxylate groups of acetate coordinate to the alkaline earth metal cations at the surfaces of the nucleators, which then leads to nucleation and crystal growth of SAT. In this context, it is worth mentioning that calcium acetate monohydrate did not act as a nucleating agent for SAT, as shown in Figure 3. A possible reason for this finding is that the local geometries of the acetate anions at the heterogeneous interface are not capable of promoting crystal growth of SAT. Calcium carbonate (calcite) was also not able to crystallize SAT, which could be due to either inaccessible calcium cations at the interface or unsuitable coordination geometries of acetate. In this context, it is also worth mentioning that there are no apparent matches of lattice constants between SAT and $CaCl_2·2H_2O$/$MgCl_2·6H_2O$.[53,54,58,59] We also analyzed the crystal structures of $CaCl_2·2H_2O$[58] and $MgCl_2·6H_2O$[59] with respect to the shortest distances between the alkaline earth metal cations and compared them with the oxygen−oxygen and carbon−carbon distances of the carboxylate groups in SAT.[53,54] Again, these analyses did not yield any obvious matches. As discussed earlier, the heterogeneous nucleation events may be caused by defect structures or reconstructed surfaces, which are difficult to derive from the bulk crystal structures. Ultimately, the nucleation processes at the heterogeneous interfaces may be understood only with the help of molecular dynamics simulations. But also, liquid-phase atomic force microscopy has recently made advances characterizing the atomic structures of solid/liquid interfaces.[64]

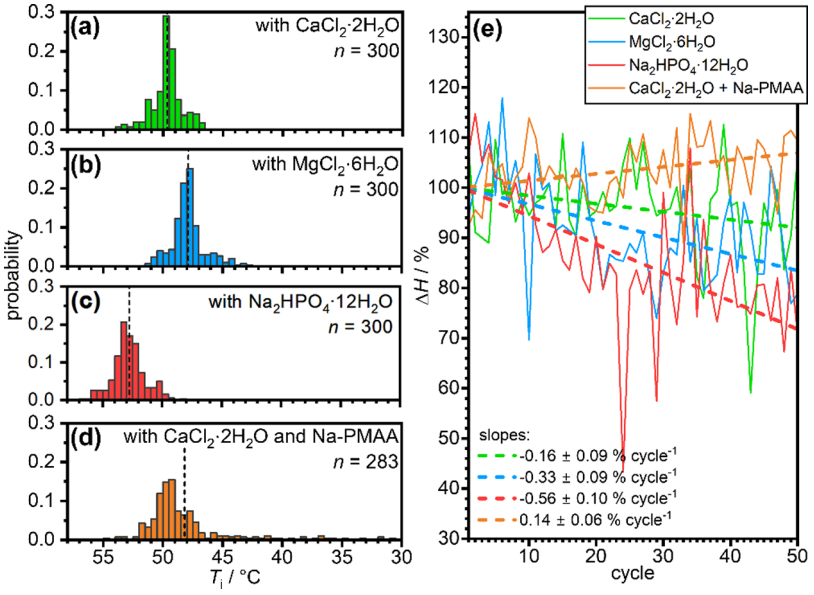


**Figure 8.** (a) Onset temperatures of crystallization of 5 g of sodium acetate with 0.250 g (4.76 wt %) of (a) $CaCl_2·2H_2O$, (b) $MgCl_2·6H_2O$, and (c) $Na_2HPO_4·12H_2O$ as the nucleating agents upon cooling at 0.5 °C min$^{-1}$ from 65 to 25 °C for 50 cycles and using 6 heating modules. The crystallization temperatures in (d) were obtained after adding 0.116 g of 30 wt % Na-PMAA polymer and 0.095 g of water as described in ref 27. The vertical dashed lines in (a−d) indicate the average temperatures. (e) Average heat releases from the 6 heating modules as the number of cycles increases to 50. Linear fits indicate the change of performance of the phase-change material using different nucleating agents. The heat releases are expressed as percentage, where 100% was defined as the intercept of the linear fits.



https://doi.org/10.1021/acs.cgd.4c00691
Cryst. Growth Des. 2024, 24, 8292−8300

In a final step, the long-term performance of $CaCl_2·2H_2O$ as a nucleating agent was benchmarked against $MgCl_2·6H_2O$ and $Na_2HPO_4·12H_2O$. These experiments were performed with maximum temperatures of 65 °C since the latter two nucleating agents would not work reliably otherwise. The experiments consisted of 50 heating/cooling cycles to test if the heat releases decrease upon thermal cycling. Such degradation effects limit the lifetime of heat batteries and need to be minimized as much as possible. For each of the nucleating agents, six samples were run in parallel, which gives in total 300 cooling scans. The complete data from one module using $CaCl_2·2H_2O$ as the nucleating agent are shown in Figure S9.

The onset temperatures, $T_i$, of the crystallization exotherms (see Figure 2(c) for a definition) did not show systematic changes with respect to the number of cycles. The various data sets including 300 individual experiments were therefore analyzed with the help of histograms as shown in Figure 8(a−c). $Na_2HPO_4·12H_2O$ displays the highest onset temperatures, with an average $T_i$ of 52.8 °C. This is followed by $CaCl_2·2H_2O$ and $MgCl_2·6H_2O$, with average $T_i$ values of 49.7 and 47.9 °C, respectively. Panel (d) in Figure 8 shows the onset temperatures using $CaCl_2·2H_2O$ as the nucleating agent with the addition of Na-PMAA polymer as described in ref 27 to prevent the formation of SAA. The nucleation events were observed most frequently just below 50 °C, as observed for the experiments without polymer in (a). However, for 17 out of 300 crystallization experiments, supercooling was observed, and therefore, no heat releases were detected.

The areas of the various exotherms are shown as a function of the cycle number in Figure 8(e). The data are somewhat noisy. However, the error analysis of the slopes of the data without polymer addition shows that they are all negative outside of the margins of error. This indicates a degradation of the heat-release performance upon thermal cycling, which is most likely due to the progressive formation of SAA. The largest loss with −0.56 ± 0.10% per cycle was observed using $Na_2HPO_4·12H_2O$ as the nucleating agent. The best performance was observed for the newly found $CaCl_2·2H_2O$ nucleating agent, with a loss of −0.16 ± 0.09% per cycle. Consistent with the literature,[27] adding the Na-PMAA polymer while again using $CaCl_2·2H_2O$ as the nucleating agent improved the deterioration of the heat releases. In fact, we even obtained a slightly positive slope of 0.14 ± 0.06% per cycle.

## CONCLUSIONS

$CaCl_2·2H_2O$ is an excellent nucleating agent for SAT that remains active even after heating to 80 °C. Reliable performance is observed above 0.1 wt %. $MgCl_2·6H_2O$ on the other hand loses its ability to nucleate SAT after heating to 80 °C. However, using a maximum temperature of 65 °C, a reliable performance was observed. In terms of degradation of the heat releases with increasing numbers of duty cycles, both $CaCl_2·2H_2O$ and $MgCl_2·6H_2O$ were found to display better characteristics compared to the commonly used $Na_2HPO_4·12H_2O$ nucleating agent. However, $CaCl_2·2H_2O$ and $MgCl_2·6H_2O$ showed more supercooling than $Na_2HPO_4·12H_2O$, with the average nucleating temperatures lowered by 3.1 and 4.9 °C, respectively. Using the Na-PMAA polymer as an additive,[27] the degradation of heat releases upon thermal cycling with $CaCl_2·2H_2O$ as nucleation agent could be stopped.

Extensive screening and performance testing of nucleating agents for SAT were possible with the new HeatMaster instrument. As part of this work, more than 1300 individual crystallization experiments were conducted. Being able to measure samples on the gram scale bridges an important gap between the milligram scale of differential scanning calorimetry and the kilogram scale of commercial heat batteries. The HeatMaster's ability to measure several samples in parallel allows a high throughput of samples and obtaining good statistics with respect to the onset temperatures and transition enthalpies. The HeatMaster's design is easily scalable, and future versions could include many more than six calorimeters. The major cost per module is the power supply, around $100. Furthermore, the HeatMaster could be easily integrated in a fully automated workflow including sample preparation, data analysis, and data interpretation with the use of machine learning. Such an approach could lead to the discovery of new high-performance phase-change materials, nucleating agents, and new strategies for improving their thermal conductivities.

## ASSOCIATED CONTENT

### Supporting Information

The Supporting Information is available free of charge at https://pubs.acs.org/doi/10.1021/acs.cgd.4c00691.

Additional experimental data showing the characteristics of the HeatMaster as well as additional nucleating experiments (PDF)

## AUTHOR INFORMATION


### Corresponding Author

**Christoph G. Salzmann** − *Department of Chemistry, University College London, London WC1H 0AJ, United Kingdom*; orcid.org/0000-0002-0714-7342; Phone: +44 7679 8864; Email: c.salzmann@ucl.ac.uk

### Authors

**Jinjie Li** − *Department of Chemistry, University College London, London WC1H 0AJ, United Kingdom*

**Michael A. Parkes** − *Department of Chemistry, University College London, London WC1H 0AJ, United Kingdom*; orcid.org/0000-0002-2958-317X

Complete contact information is available at: https://pubs.acs.org/10.1021/acs.cgd.4c00691


### Notes

The authors declare no competing financial interest.

## ACKNOWLEDGMENTS

We thank Tony Bernard for help with the soldering of electronic components, Angelo Delbusso for machining the aluminum parts, Martin Vickers for providing training using the X-ray diffraction instrument, and Jamie Gould for providing calibration data of the X-ray diffractometer.

## REFERENCES

(1) Sharma, S. D.; Sagara, K. Latent Heat Storage Materials and Systems: A Review. *Int. J. Green Energy* **2005**, *2*, 1−56.

(2) Kiyabu, S.; Girard, P.; Siegel, D. J. Discovery of Salt Hydrates for Thermal Energy Storage. *J. Am. Chem. Soc.* **2022**, *144*, 21617−21627.

(3) Odoi-Yorke, F.; Opoku, R.; Davis, F.; Obeng, G. Y. Optimisation of thermal energy storage systems incorporated with phase change materials for sustainable energy supply: A systematic review. *Energy Rep.* **2023**, *10*, 2496−2512.

(4) Liu, L.; Zhang, Y.; Zhang, S.; Tang, B. Advanced Phase Change Materials from Natural Perspectives: Structural Design and Functional Applications. *Adv. Sci.* **2023**, *10*, 2207652.
(5) Matuszek, K.; Kar, M.; Pringle, J. M.; MacFarlane, D. R. Phase Change Materials for Renewable Energy Storage at Intermediate Temperatures. *Chem. Rev.* **2023**, *123*, 491−514.
(6) Piper, S. L.; Forsyth, C. M.; Kar, M.; Gassner, C.; Vijayaraghavan, R.; Mahadevan, S.; Matuszek, K.; Pringle, J. M.; MacFarlane, D. R. Sustainable materials for renewable energy storage in the thermal battery. *RSC Sustain.* **2023**, *1*, 470−480.
(7) Chen, Y.; Xu, P.; Chen, Z.; Wang, H.; Sha, H.; Ji, Y.; Zhang, Y.; Dou, Q.; Wang, S. Experimental investigation of demand response potential of buildings: Combined passive thermal mass and active storage. *Appl. Energy* **2020**, *280*, 115956.
(8) Rozanna, D.; Chuah, T. G.; Salmiah, A.; Choong, T. S. Y.; Sa'ari, M. Fatty Acids as Phase Change Materials (PCMs) for Thermal Energy Storage: A Review. *Int. J. Green Energy* **2005**, *1*, 495−513.
(9) Purohit, B. K.; Sistla, V. S. Inorganic salt hydrate for thermal energy storage application: A review. *Energy Storage* **2021**, *3*, No. e212.
(10) Khadiran, T.; Hussein, M. Z.; Zainal, Z.; Rusli, R. Advanced energy storage materials for building applications and their thermal performance characterization: A review. *Renew. Sustain. Energy Rev.* **2016**, *57*, 916−928.
(11) Kenisarin, M.; Mahkamov, K. Salt hydrates as latent heat storage materials: Thermophysical properties and costs. *Sol. Energy Mater. Sol. Cells* **2016**, *145*, 255−286.
(12) Alva, G.; Liu, L.; Huang, X.; Fang, G. Thermal energy storage materials and systems for solar energy applications. *Renew. Sustain. Energy Rev.* **2017**, *68*, 693−706.
(13) Wang, Z.; Liu, S.; Ma, G.; Xie, S.; Du, G.; Sun, J.; Jia, Y. Preparation and properties of caprylic-nonanoic acid mixture/expanded graphite composite as phase change material for thermal energy storage. *Int. J. Energy Res.* **2017**, *41*, 2555−2564.
(14) Naumann, R.; Emons, H. H. Results of thermal analysis for investigation of salt hydrates as latent heat-storage materials. *J. Therm. Anal.* **1989**, *35*, 1009−1031.
(15) Sharma, A.; Tyagi, V. V.; Chen, C. R.; Buddhi, D. Review on thermal energy storage with phase change materials and applications. *Renew. Sustain. Energy Rev.* **2009**, *13*, 318−345.
(16) Beaupere, N.; Soupremanien, U.; Zalewski, L. Nucleation triggering methods in supercooled phase change materials (PCM), a review. *Thermochim. Acta* **2018**, *670*, 184−201.
(17) Cabeza, L. F.; Svensson, G.; Hiebler, S.; Mehling, H. Thermal performance of sodium acetate trihydrate thickened with different materials as phase change energy storage material. *Appl. Therm. Eng.* **2003**, *23*, 1697−1704.
(18) Mao, J.; Dong, X.; Hou, P.; Lian, H. Preparation research of novel composite phase change materials based on sodium acetate trihydrate. *Appl. Therm. Eng.* **2017**, *118*, 817−825.
(19) Kong, W.; Dannemand, M.; Johansen, J. B.; Fan, J.; Dragsted, J.; Englmair, G.; Furbo, S. Experimental investigations on heat content of supercooled sodium acetate trihydrate by a simple heat loss method. *Sol. Energy* **2016**, *139*, 249−257.
(20) Xiao, Q.; Fan, J.; Li, L.; Xu, T.; Yuan, W. Solar thermal energy storage based on sodium acetate trihydrate phase change hydrogels with excellent light-to-thermal conversion performance. *Energy* **2018**, *165*, 1240−1247.
(21) Su, W.; Darkwa, J.; Kokogiannakis, G. Review of solid-liquid phase change materials and their encapsulation technologies. *Renew. Sustain. Energy Rev.* **2015**, *48*, 373−391.
(22) Huang, J.; Wang, T.; Zhu, P.; Xiao, J. Preparation, characterization, and thermal properties of the microencapsulation of a hydrated salt as phase change energy storage materials. *Thermochim. Acta* **2013**, *557*, 1−6.
(23) Dannemand, M.; Johansen, J. B.; Furbo, S. Solidification behavior and thermal conductivity of bulk sodium acetate trihydrate composites with thickening agents and graphite. *Sol. Energy Mater. Sol. Cells* **2016**, *145*, 287−295.
(24) Lizana, J. C. R.; Barrios-Padura, A.; Valverde, J. M.; Ortiz, C. Identification of best available thermal energy storage compounds for low-to-moderate temperature storage applications in buildings. *Mater. Construcc.* **2018**, *68*, No. e160.
(25) Lizana, J.; Sanchez-Jimenez, P. E.; Chacartegui, R.; Becerra, J. A.; Perez-Maqueda, L. A. Supercooled sodium acetate aqueous solution for long-term heat storage to support heating decarbonisation. *J. Energy Storage* **2022**, *55*, 105584.
(26) Pebler, A. Dissociation vapor pressure of sodium acetate trihydrate. *Thermochim. Acta* **1975**, *13*, 109−114.
(27) Oliver, D. E.; Bissell, A. J.; Liu, X.; Tang, C. C.; Pulham, C. R. Crystallisation studies of sodium acetate trihydrate - suppression of incongruent melting and sub-cooling to produce a reliable, high-performance phase-change material. *CrystEngComm* **2021**, *23*, 7−76.
(28) Guion, J.; Teisseire, M. Nucleation of sodium acetate trihydrate in thermal heat storage cycles. *Sol. Energy* **1991**, *46*, 97−100.
(29) Wada, T.; Matsuo, Y. Studies on Salt Hydrates for Latent Heat Storge. VI. Preheating Effect on Crystallization of Sodium Acetate Trihydrate from Aqueous Solution with a Small Amount of Disodium Hydrogenphosphate. *Bull. Chem. Soc. Jpn.* **1984**, *57*, 561−563.
(30) Kumar, N.; Hirschey, J.; LaClair, T. J.; Gluesenkamp, K. R.; Graham, S. Review of stability and thermal conductivity enhancements for salt hydrates. *J. Energy Storage* **2019**, *24*, 100794.
(31) Wada, T.; Yamamoto, R.; Matsuo, Y. Heat storage capacity of sodium acetate trihydrate during thermal cycling. *Sol. Energy* **1984**, *33*, 373−375.
(32) Green, W. F. The "Melting-Point" of Hydrated Sodium Acetate: Solubility Curves. *J. Phys. Chem.* **1908**, *12*, 655−660.
(33) Wada, T.; Yamamoto, R. Studies on Salt Hydrate for Latent Heat Storage. I. Crystal Nucleation of Sodium Acetate Trihydrate Catalyzed by Tetrasodium Pyrophosphate Decahydrate. *Bull. Chem. Soc. Jpn.* **1982**, *55*, 3603−3606.
(34) Mao, J.; Hou, P.; Liu, R.; Chen, F.; Dong, X. Preparation and thermal properties of SAT-CMC-DSP/EG composite as phase change material. *Appl. Therm. Eng.* **2017**, *119*, 585−592.
(35) Ryu, H. W.; Woo, S. W.; Shin, B. C.; Kim, S. D. Prevention of supercooling and stabilization of inorganic salt hydrates as latent heat storage materials. *Sol. Energy Mater. Sol. Cells* **1992**, *27*, 161−172.
(36) Li, X.; Zhou, Y.; Nian, H.; Zhu, F.; Ren, X.; Dong, O.; Hai, C.; Shen, Y.; Zeng, J. Preparation and thermal energy storage studies of CH3COONa·3$H_2$O-KCl composites salt system with enhanced phase change performance. *Appl. Therm. Eng.* **2016**, *102*, 708−715.
(37) Cui, W.; Yuan, Y.; Sun, L.; Cao, X.; Yang, X. Experimental studies on the supercooling and melting/freezing characteristics of nano-copper/sodium acetate trihydrate composite phase change materials. *Renew. Energy* **2016**, *99*, 1029−1037.
(38) Garay Ramirez, B. M. L.; Glorieux, C.; San Martin Martinez, E.; Flores Cuautle, J. J. A. Tuning of thermal properties of sodium acetate trihydrate by blending with polymer and silver nanoparticles. *Appl. Therm. Eng.* **2014**, *62*, 838−844.
(39) Hu, P.; Lu, D.-J.; Fan, X.-Y.; Zhou, X.; Chen, Z.-S. Phase change performance of sodium acetate trihydrate with AlN nanoparticles and CMC. *Sol. Energy Mater. Sol. Cells* **2011**, *95*, 2645−2649.
(40) Liu, C.; Hu, P.; Xu, Z.; Ma, X.; Rao, Z. Experimental investigation on thermal properties of sodium acetate trihydrate based phase change materials for thermal energy storage. *Thermochim. Acta* **2019**, *674*, 28−35.
(41) Stunić, Z.; Djuričković, V.; Stunić, Z. Thermal storage: Nucleation of melts of inorganic salt hydrates. *J. Appl. Chem. Biotechnol.* **1978**, *28*, 761−764.
(42) Fashandi, M.; Leung, S. N. Sodium acetate trihydrate-chitin nanowhisker nanocomposites with enhanced phase change performance for thermal energy storage. *Sol. Energy Mater. Sol. Cells* **2018**, *178*, 259−265.
(43) Dannemand, M.; Dragsted, J.; Fan, J.; Johansen, J. B.; Kong, W.; Furbo, S. Experimental investigations on prototype heat storage units utilizing stable supercooling of sodium acetate trihydrate mixtures. *Appl. Energy* **2016**, *169*, 72−80.


https://doi.org/10.1021/acs.cgd.4c00691
*Cryst. Growth Des.* 2024, 24, 8292−8300

(44) Vekilov, P. G. The two-step mechanism of nucleation of crystals in solution. *Nanoscale* **2010**, *2*, 2346−2357.
(45) Bai, G.; Gao, D.; Liu, Z.; Zhou, X.; Wang, J. Probing the critical nucleus size for ice formation with graphene oxide nanosheets. *Nature* **2019**, *576*, 437−441.
(46) Kumar, N.; Banerjee, D. Thermal Cycling of Calcium Chloride Hexahydrate With Strontium Chloride as a Phase Change Material for Latent Heat Thermal Energy Storage Applications in a Non-differential Scanning Calorimeter Set-Up. *J. Thermal Sci. Eng. Appl.* **2019**, *11*, DOI: 10.1115/1.4042859.
(47) Dunn, T. H.; Skaanvik, S. A.; McPherson, I. J.; O'Shaughnessy, C.; He, X.; Kulak, A. N.; Micklethwaite, S.; Matamoros-Veloza, A.; Sandei, I.; Hunter, L.; et al. Universality of Hair as a Nucleant: Exploring the Effects of Surface Chemistry and Topography. *Cryst. Growth Des.* **2023**, *23*, 8978−8990.
(48) Holden, M. A.; Whale, T. F.; Tarn, M. D.; O'Sullivan, D.; Walshaw, R. D.; Murray, B. J.; Meldrum, F. C.; Christenson, H. K. High-speed imaging of ice nucleation in water proves the existence of active sites. *Science Adv.* **2019**, *5*, eaav4316.
(49) Kenfack, F.; Bauer, M. Innovative Phase Change Material (PCM) for Heat Storage for Industrial Applications. *Energy Procedia* **2014**, *46*, 310−316.
(50) Leys, J.; Duponchel, B.; Longuemart, S.; Glorieux, C.; Thoen, J. A new calorimetric technique for phase change materials and its application to alkane-based PCMs. *Mater. Renew. Sustain. Energy* **2016**, *5*, 4.
(51) Lazerges, M.; Rietveld, I. B.; Corvis, Y.; Céolin, R.; Espeau, P. Thermodynamic studies of mixtures for topical anesthesia: Lidocaine-salol binary phase diagram. *Thermochim. Acta* **2010**, *497*, 124−128.
(52) *GSAS - General Structure Analysis System*; University of California, 1985.
(53) Cameron, T. S.; Mannan, K. M.; Rahman, M. O. The crystal structure of sodium acetate trihydrate. *Acta Crystallogr.* **1976**, *B32*, 87−90.
(54) Wei, K.-T.; Ward, D. L. Sodium acetate trihydrate: a redetermination. *Acta Crystallogr.* **1977**, *B33*, 522−526.
(55) Hsu, L.-Y.; Nordman, C. E. Structures of two forms of sodium acetate, $Na^{+}.C2H3O2^{-}$. *Acta Crystallogr.* **1983**, *C39*, 690−694.
(56) Helmholdt, R. B.; Sonneveld, E. J.; Schenk, H. Ab initio crystal structure determination of $\beta$-sodium acetate from powder data. *Z. Kristallogr.* **1998**, *213*, 596−598.
(57) Dittrich, B.; Bergmann, J.; Roloff, P.; Reiss, G. J. New polymorphs of the phase-change material sodium acetate. *Crystals* **2018**, *8*, 213.
(58) Leclaire, A.; Borel, M. M. Le dichlorure de calcium dihydrate. *Acta Cryst. B* **1977**, *33*, 1608−1610.
(59) Agron, P. A.; Busing, W. R. Magnesium dichloride hexahydrate, MgCl2.6H2O, by neutron diffraction. *Acta Cryst. C* **1985**, *41*, 8−10.
(60) Baumgartner, M.; Bakker, R. J. $CaCl_2$-hydrate nucleation in synthetic fluid inclusions. *Chem. Geol.* **2009**, *265*, 335−344.
(61) Brady, J. B. Magma in a beaker: Analog Experiments with water and various salts or sugar for teaching igneous petrology. *Canad. Mineral.* **2009**, *47*, 457−471.
(62) Marcus, Y.; Dangor, V.; Lessery, S. The phase diagram of magnesium bromide and chloride hexahydrate mixtures. *Thermochim. Acta* **1984**, *77*, 219−226.
(63) Cantor, S. DSC study of melting and solidification of salt hydrates. *Thermochim. Acta* **1979**, *33*, 69−86.
(64) Dickbreder, T.; Sabath, F.; Reischl, B.; Nilsson, R. V. E.; Foster, A. S.; Bechstein, R.; Kühnle, A. Atomic structure and water arrangement on K-feldspar microcline (001). *Nanoscale* **2024**, *16*, 3462−3473.



https://doi.org/10.1021/acs.cgd.4c00691
*Cryst. Growth Des.* 2024, 24, 8292−8300